2013

Optical studies of strain and defect distribution in semipolar (1(1)over-bar01) GaN on patterned Si substrates

N. Izyumskaya
Virginia Commonwealth University, nizioumskaia@vcu.edu

F. Zhang
Virginia Commonwealth University

S. Okur
Virginia Commonwealth University, okurs@vcu.edu

See next page for additional authors

Izyumskaya, N., Zhang, F., & Okur, S., et al. Optical studies of strain and defect distribution in semipolar (1(1)over-bar01) GaN on patterned Si substrates. Journal of Applied Physics, 114, 113502 (2013).

JOURNAL OF APPLIED PHYSICS **114**, 113502 (2013)

Optical studies of strain and defect distribution in semipolar $(1\bar{1}01)$ GaN on patterned Si substrates

N. Izyumskaya,[1,a)] F. Zhang,[1] S. Okur,[1] T. Selden,[1] V. Avrutin,[1] Ü. Özgür,[1] S. Metzner,[2] C. Karbaum,[2] F. Bertram,[2] J. Christen,[2] and H. Morkoç[1]
[1]*Department of Electrical and Computer Engineering, Virginia Commonwealth University, Richmond, Virginia 23284, USA*
[2]*Institute of Experimental Physics, Otto-von-Guericke-University Magdeburg, Magdeburg D-39106, Germany*

(Received 8 February 2013; accepted 2 September 2013; published online 16 September 2013)

Formation of defects in semipolar $(1\bar{1}01)$-oriented GaN layers grown by metal-organic chemical vapor deposition on patterned Si (001) substrates and their effects on optical properties were investigated by steady-state and time-resolved photoluminescence (PL) and spectrally and spatially resolved cathodoluminescence (CL). Near-band edge emission is found to be dominant in the c^+-wings of semipolar $(1\bar{1}01)$GaN, which are mainly free from defect-related emission lines, while the c^- wings contain a large number of basal stacking faults. When the advancing c^+ and c^- fronts meet to coalesce into a continuous film, the existing stacking faults contained in c^- wings continue to propagate in the direction perpendicular to the c-axis and, as a result, the region dominated by stacking fault emission is extended to the film surface. Additional stacking faults are observed within the $c+$ wings, where the growing c^+ wings of GaN are in contact with the SiO_2 masking layer. Out-diffusion of oxygen/silicon species and concentration of strain near the contact region are considered as possible causes of the stacking fault formation. CL linescans performed along the surface and across the thickness of the non-coalesced and coalesced layers revealed that, while most of the material in the near-surface region of the non-coalesced layers is relaxed, coalescence results in nonuniform strain distribution over the layer surface. Red-shifted near-band-edge emission from the near-surface region indicates tensile stress near the surface of a coalesced layer, reaching a value of 0.3 GPa. The regions near the GaN/AlN/Si(111) interface show slightly blue shifted, broadened near-band-edge emission, which is indicative of a high concentration of free carriers possibly due to incorporation of shallow-donor impurities (Si and/or O) from the substrate or SiO_2 mask. Steady-state and time-resolved PL results indicate that semipolar $(1\bar{1}01)$GaN on patterned Si exhibits optical properties (PL intensity and carrier lifetimes) approaching to those of the state-of-the-art c-plane GaN grown using *in situ* SiN_x nanonetwork mask on c-plane sapphire. Long PL lifetimes ($\sim$2 ns) for the $(1\bar{1}01)$GaN layers show that the semipolar material holds promise for light emitting and detecting devices. © *2013 AIP Publishing LLC*. [http://dx.doi.org/10.1063/1.4821343]

I. INTRODUCTION

GaN-based materials have had an unparalleled impact on blue and green light emitting diodes (LEDs) to help produce full color displays together with the InGaAsP-based red variety.[1] However, efficiencies and output power levels must be increased as well as cost reduced for insertion in lighting technology fuelled by long operating lifetimes, reduced carbon footprint, and lower maintenance cost.[2] The workhorse for these LEDs has been the basal plane (c-plane) GaN grown on c-plane sapphire and/or basal-plane SiC and in limited cases GaN substrates. The c [0001] axis of wurtzite GaN is electrically polar; adversely affecting device performance through spontaneous (composition-induced) and piezoelectric (strain-induced) polarization. Polarization field causes spatial separation of electron and hole wave functions in quantum wells (QWs), which make up the active regions of LEDs and also laser diodes (LDs), reducing the quantum efficiency, particularly at low injection levels.[3–5] Thin QWs are usually used to mitigate this problem somewhat, but at the expense of reduced total density of available states, and thus reduced light output. Increasing the number of QWs is also problematic because not all of the wells may be populated equally under electrical injection, particularly by holes due to their large effective mass. Additionally, the quantum confined Stark effect leads to red shift of emission wavelength, the extent of which depends on the carrier injection level due to varying degrees of screening. To fully screen the polarization charge, a density of injected carriers on the order of 10^{19} cm^{-3} is required.

In contrast, nonpolar orientations have no polarization charge at interfaces. Theoretical calculations[6] predict that the piezoelectric field across GaInN/GaN heterostructures would be considerably reduced in semipolar orientations as well. These predictions have fueled efforts to explore wurtzite GaN of various semipolar orientations. Heretofore, the growth of $(1\bar{1}01)$ and $(1\bar{1}03)$ GaN on spinel,[7] $(1\bar{1}03)$ and $(11\bar{2}2)$ GaN on m-plane sapphire,[8,9] $(11\bar{2}2)$ GaN on bulk GaN,[10] $(1\bar{1}01)$ GaInN/GaN QWs on patterned $(1\bar{1}02)$ SiC,[11] and $(1\bar{1}01)$ and $(11\bar{2}2)$GaN on patterned Si substrates[12,13] has been reported. In agreement with predictions, the electric field across semipolar InGaN/GaN QWs was found to be

[a)]Author to whom correspondence should be addressed. Electronic mail: nizioumskaia@vcu.edu

weaker than that for the *c*-orientation,[14,15] but naturally stronger than that for the nonpolar variety.[16] In spite of the observed reduction of the piezoelectric field in semipolar InGaN/GaN QWs and elimination of the field in the nonpolar material, the efficiency of nonpolar and semipolar LEDs still lags behind that of *c*-plane GaN plausibly due to low crystal quality of semipolar material as compared to the *c*-plane GaN.[17,18] The said inferior crystal quality is attributed to a high density of extended defects, mainly threading dislocations and basal-plane stacking faults (BSFs) nucleated at the GaN/substrate interface.[19,20] Note that, in the case of nonpolar growth, *c* planes are normal to the film surface (inclined to the surface in the case of growth in a semipolar direction); therefore, SFs easily formed on the basal plane propagate throughout a growing nonpolar or semipolar film to the surface, thus deteriorating material quality. Microscopic mechanisms governing the defect formation are not well understood yet. Comprehensive studies of defect formation in nonpolar and semipolar nitrides are required for improvement of material quality and thus device performance.

Although bulk nonpolar GaN substrates are available, they are prohibitively expensive and very limited in size. Among the foreign substrates, Si is the most attractive choice due to its high quality, good thermal conductivity, low cost, wide availability, large size, and ease of selective removal before packaging. Furthermore, growth on Si substrates would also make it possible to integrate GaN-based optoelectronic devices with Si-based electronics such as the control and stabilization circuitry used in high performance LEDs. Growth of *c*-plane GaN on Si has been explored relatively extensively; however, studies of nonpolar and semipolar GaN growth on Si have been limited.[12,21,22]

Recently, we have investigated effects of metal-organic chemical vapor deposition (MOCVD) growth conditions on optical properties of $(1\bar{1}01)$GaN on patterned Si(001) substrates[13] and demonstrated that optical quality of $(1\bar{1}01)$GaN/Si is comparable to that of state-of-the-art *c*-plane GaN layers[23] established in our group using *in situ* epitaxial lateral overgrowth on a silicon nitride nano-network.[24] In this work, we expanded our investigations to the area of steady-state and time-resolved photoluminescence as well as defect and strain distribution in coalesced and non-coalesced semipolar $(1\bar{1}01)$-oriented GaN layers on patterned Si (001) substrates.

II. EXPERIMENTAL

To achieve $(1\bar{1}01)$ GaN film surface parallel to the substrate, Si(001) substrates that are miscut 7° toward the Si ⟨110⟩ direction were used. The substrates were patterned to form grooves aligned parallel to the ⟨110⟩ Si direction as described elsewhere.[13,23] The top terraces were 3 μm wide, while grooves were either 10 or 3 μm wide (hereafter, 3 μm × 10 μm and 3 μm × 3 μm patterns, respectively). A 50-nm-thick AlN layer was grown by MOCVD to serve as a seed layer for GaN growth. SiO_2 mask layer was formed on one of the sidewalls of the groove, and subsequent growth of GaN started on the opposite side of the groove. The substrates were then reloaded into the MOCVD chamber and GaN growth was performed with the use of trimethylgallium (TMG) and NH_3 as sources of Ga and N, respectively. Semipolar GaN layers were grown at a chamber pressure of 200 Torr and high NH_3 flow rates (>2000 sccm), which were found to be favorable for the $(1\bar{1}01)$ facet formation.[13,23] The growth initiated on Si{111} sidewalls free from SiO_2 and then advanced laterally first along the GaN [0001] c^+ direction and then additionally along the $[000\bar{1}]$ c^- direction after the vertical growth advanced above the Si(001) terraces.

Morphology and structural properties of the GaN layers were studied by scanning electron microscopy (SEM), atomic force microscopy (AFM), and x-ray diffraction (XRD). Defect distribution in the GaN stripes was examined by highly spatially and spectrally resolved cathodoluminescence (CL) using a system built around JEOL 6400 scanning electron microscope.[25] Optical quality of the semipolar material was characterized by steady-state photoluminescence (PL) and time-resolved PL (TRPL) as well as spatially resolved CL. 257–267 nm excitation from a frequency tripled Ti:Sapphire laser with a pulse width of 150 fs was used in combination with a Hamamatsu streak camera for the TRPL measurements and a 325 nm wavelength HeCd laser for steady-state PL.

III. RESULTS AND DISCUSSION

To shed light on the defects emanating at the coalescing fronts and their effect on optical properties of semipolar GaN, coalesced and non-coalesced layers were prepared. Figures 1(a) and 1(b) show SEM images of coalesced and non-coalesced $(1\bar{1}01)$ GaN layers grown in one MOCVD process on Si substrates with 3 μm × 3 μm and 3 μm × 10 μm patterns, respectively. One can see, that the film grown on the 3 μm × 3 μm patterned substrate is fully coalesced [Fig. 1(a)], while c^+ and c^- growth fronts of GaN grown with the 3 μm × 10 μm pattern are not merge together in a continuous layer [Fig. 1(b)]. From XRD data, the epitaxial relationships are GaN[0001] || Si$[\bar{1}\bar{1}1]$, GaN$[\bar{1}\bar{1}20]$ || Si$[1\bar{1}0]$, and GaN$(1\bar{1}01)$ make an angle of 7° with the Si(001) plane. Figure 2 represents an AFM image of 4 μm × 4 μm area of the film shown in Fig. 1(b). The $(1\bar{1}01)$ GaN surface parallel to substrate surface had a root-mean-square (rms) roughness of about 0.8 nm over an area of 4 × 4 μm^2 with well resolved atomic steps, suggesting a step-flow growth mode of the $(1\bar{1}01)$ plane.

A. Spatially resolved CL study of defect distribution in semipolar $(1\bar{1}01)$ GaN

To gain insight into the defect distribution in the semipolar layers, we performed spectrally and spatially resolved CL studies of coalesced and non-coalesced $(1\bar{1}01)$GaN layers at 5.8 K. Figure 3 presents the CL results for the non-coalesced layer together with its cross-sectional [Fig. 3(a)] and plan view [Fig. 3(d)] SEM images. CL intensity is considerably reduced at the GaN/Si interface (where the growth starts) due to non-radiative recombination on threading dislocations[26] propagating in the c^+ direction [see Figs. 3(b) and 3(e)]. The spotty dark regions in the plan view of

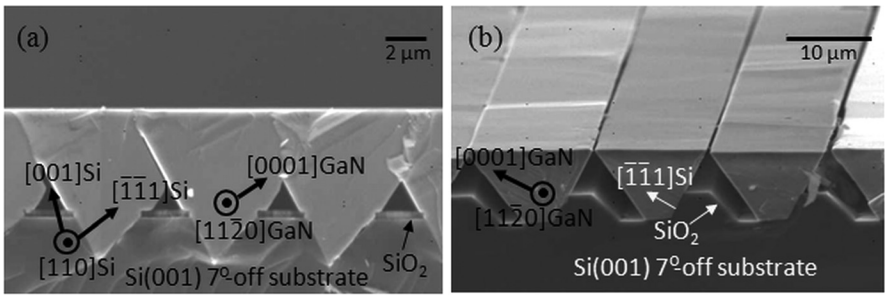

FIG. 1. (a) Cross-sectional SEM image of coalesced $(1\bar{1}01)$GaN layer grown on Si(001) substrate with 3 μm × 3 μm pattern and (b) inclined SEM image of non-coalesced layer grown on Si(001) substrate with 3 μm × 10 μm pattern.

Fig. 3(e) correspond to projection of the c^- wing on the $(1\bar{1}01)$GaN surface, and dark lines extending into the c^+ wing are projections of the threading dislocations. As seen from the CL wavelength images [Figs. 3(c) and 3(f)], emission at about 362 nm related to BSFs[27–29] is observed from the c^- wing, in agreement with our data reported earlier.[23] In contrast, no BSF emission is observed from the c^+ wing region, where the (D^0, X) GaN emission dominates. It should be noted that the 361-nm emission emanating from the bottom facet of the c^+-wing [shown with green color in Fig. 3(c)] does not have a BSF origin, as it peaks at a wavelength 2–3 nm shorter than that characteristic of the BSF emission, but is most likely red-shifted near-band-edge (NBE) band. The red shift is caused the fact that excitation conditions in this place are dramatically different: contrary to nearly normal incidence of the electron beam on the sample cross-section; in this case, the electron beam is nearly parallel to the bottom facet of the c^+-wing.

Figure 4 shows spectrally and spatially resolved CL images from a coalesced GaN layer together with an SEM image. It is evident from the CL data that when c^+ and c^- fronts meet and the growing material coalesces into the continuous film, the existing defects, e.g., BSFs continue to propagate in the direction perpendicular to the c-axis and, as a result, the region dominated with BSF emission is extended to the film surface [Fig. 4(c)]. Several luminescence channels between 362 nm and 380 nm are observed, which is indicative of the presence of several types of BSFs, prismatic SFs, partial dislocations (PDs), donor-acceptor pairs (DAPs) in the c^- wings. No additional optically active defects were found at the coalescence fronts.

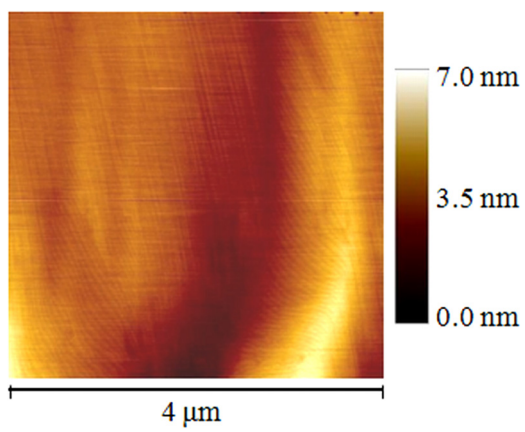

FIG. 2. AFM image of 4 μm × 4 μm area of the c^+ wing of semipolar $(1\bar{1}01)$ GaN shown in Fig. 1(b); vertical range is 7 nm, and the rms roughness is 0.8 nm.

Another interesting finding is the formation of BSFs within the c^+ wings, where the growing c^+ wings of GaN make contact with the SiO_2 masking layer [see Fig. 4(c)]. As in the case of BSFs within the c^- wings, these BSFs are normal to the c-direction of GaN and form additional BSF "rows" within the c^+ wings. As mentioned in Sec. II, the grooves in Si substrates are either 10 or 3 μm wide by design. In the case of 10-μm wide grooves, GaN grows free in the c^+ direction until the c^+ and c^- wings meet, as seen in the SEM image on Fig. 1(b). In the case of the narrower, 3-μm wide grooves, the c^+ wings make contact the SiO_2 masking layer on the top terraces, as seen in Fig. 1(a). Figure 5(b) shows schematically the shape evolution of the growing GaN fronts in the latter case. One can see that initially the GaN stripe grows freely in all directions, but eventually the c^+ growth front comes in contact with the SiO_2 masking layer, which results in the formation of BSFs lying in the basal planes. Concentration of strain near the contact region and/or oxygen and/or silicon out-diffusion from SiO_2 followed by surface migration of the species could be considered as possible causes of this BSF formation. A similar mechanism may be responsible for the formation of stacking faults in c^- wings, which is in permanent contact with the SiO_2 mask during growth. Further microscopic investigation is warranted to clarify origin of the BSFs. Note that since the Si (001) substrate has 7°-miscut toward the Si ⟨110⟩ direction, the c^+ and c^- wings are located at the same level at the meeting fronts, which is not favorable for the overgrowth of c^+ wings over c^- wings. As the result, upon coalescence the continuous $(1\bar{1}01)$ top surface forms and further growth proceeds normal to the $(1\bar{1}01)$ plane. Under these conditions, BSFs, once formed, terminate on the growing surface and extend further with the growing surface, and the introduction of additional layers, e.g., low-temperature AlN or AlGaN,[30] is required for BSF termination.

B. Steady-state and time-resolved PL measurements

Figure 6 shows PL spectra and transients for the coalesced and non-coalesced $(1\bar{1}01)$GaN layers grown on the Si(001)7°-off substrates with 3 μm × 3 μm and 3 μm × 10 μm groove patterns, respectively. For reference, Fig. 6 displays also optical data for a c-plane GaN/sapphire template and a c-plane GaN layer grown on the state-of-art GaN templates using *in situ* epitaxial lateral overgrowth (ELO) with a SiN_x nano-network mask that blocks dislocation propagation (referred to as nano-ELO layer).[24] As seen from Fig. 6(a), the intensity of NBE from the non-coalesced $(1\bar{1}01)$ GaN is comparable to that from the c-plane reference GaN

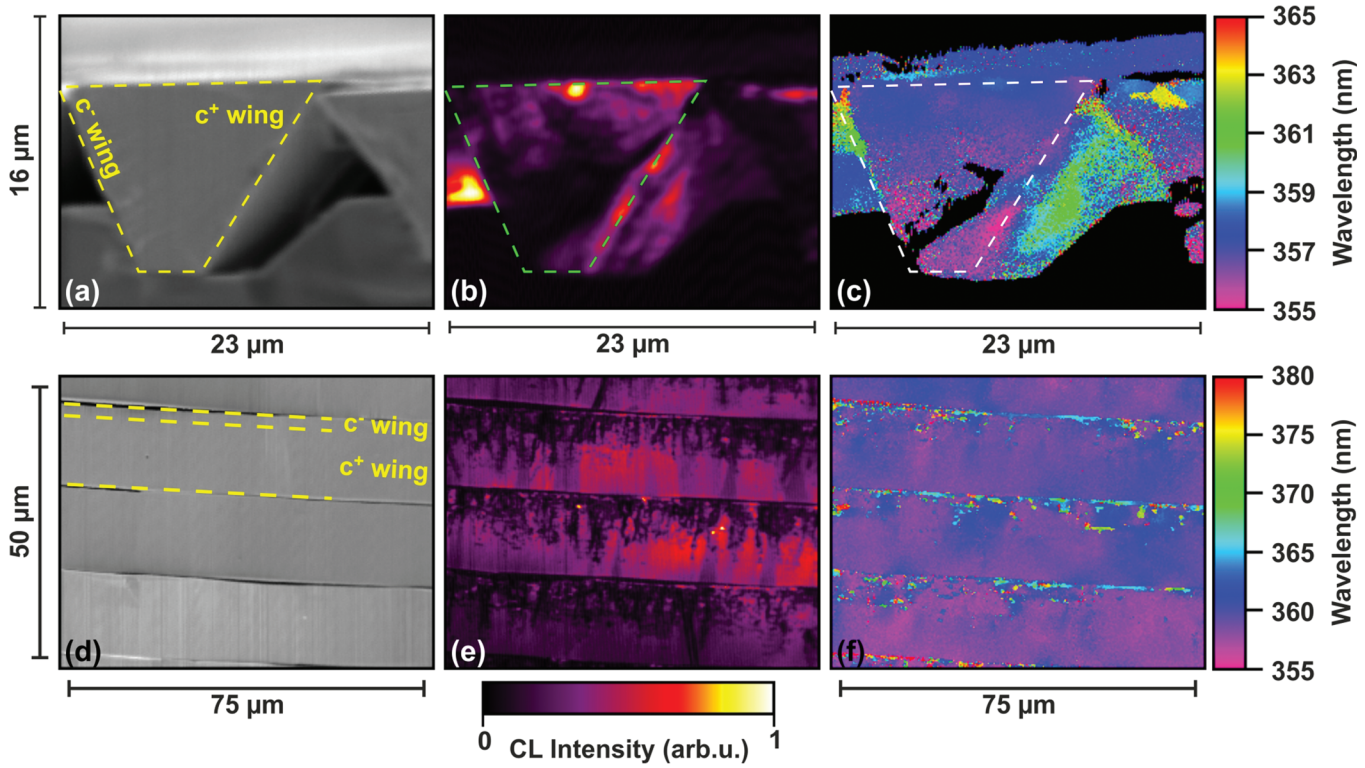

FIG. 3. (a) Cross-sectional and (d) top-view SEM images of non-coalesced $(1\bar{1}01)$ GaN layer and corresponding (b) and (e) integral CL intensity images and (c) and (f) CL wavelength images, showing spatial peak wavelength distribution.

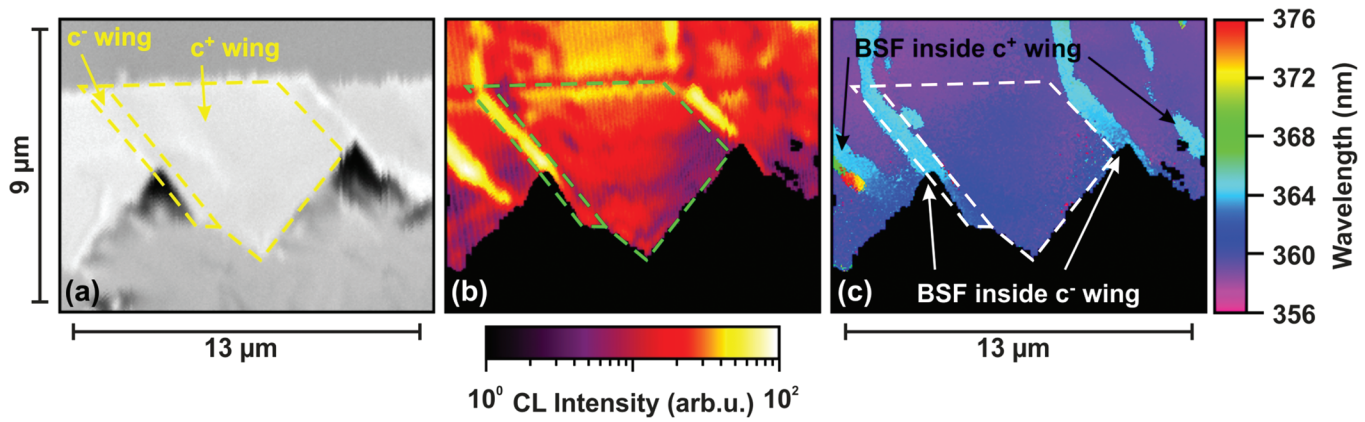

FIG. 4. (a) Cross-sectional inclined SEM image of coalesced $(1\bar{1}01)$ GaN layer and the corresponding (b) integral CL intensity images on logarithmic scale and (c) CL peak wavelength image.

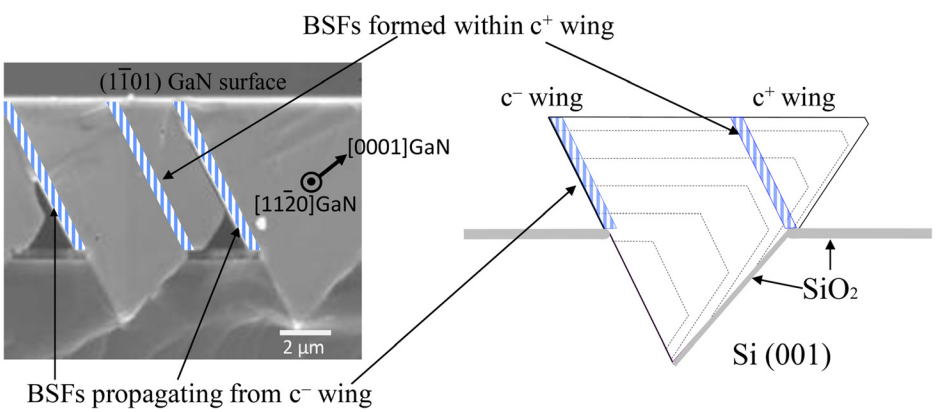

FIG. 5. (Left) cross-sectional SEM image of a coalesced $(1\bar{1}01)$ GaN layer on Si(001), with schematic illustrating BSF-containing regions within c^+ wings (dashed regions) and (right) schematic sketch of GaN growth progression for the case when a c^+ wings contacts the SiO_2 mask. Dashed lines marking the $(1\bar{1}01)$ and (0001) growth planes reflect the growth rate ratio obtained experimentally. Bottom $(1\bar{1}01)$ growth front propagates with very low rate due to limited material supply.

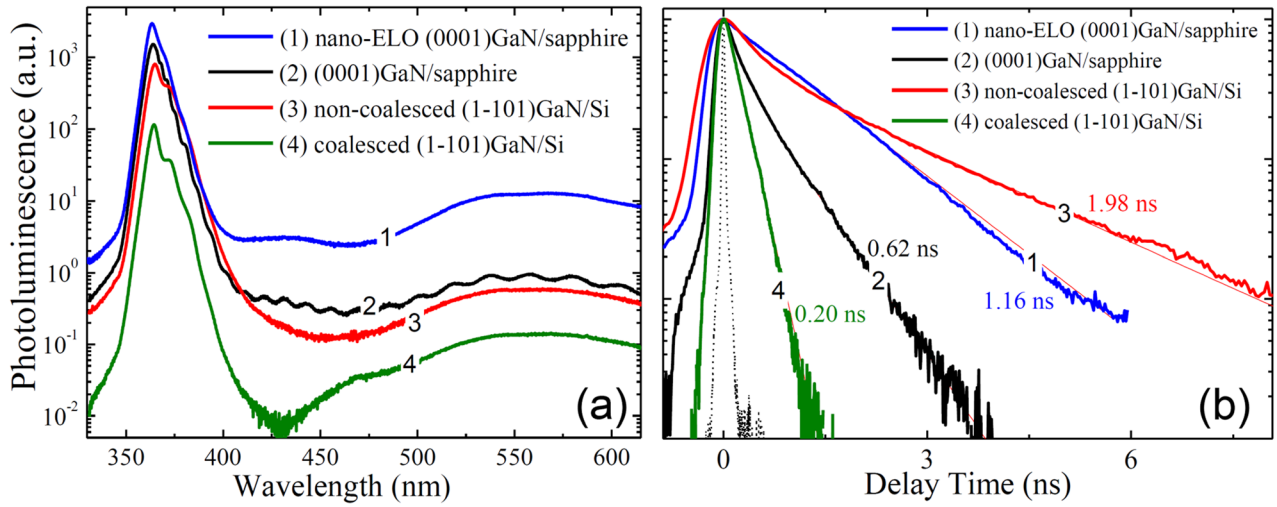

FIG. 6. (a) Room-temperature steady-state PL spectra for coalesced (curve 4) and non-coalesced (curve 3) semipolar $(1\bar{1}01)$GaN layers in comparison with *c*-plane GaN/sapphire template (curve 2) and state-of-art *c*-plane GaN templates prepared by *in situ* ELO using SiN_x nano-network (curve 1). Excitation density is 0.032 kW/cm^2. Background is subtracted from the spectra. (b) Room-temperature TRPL results for coalesced (curve 4) and non-coalesced (curve 3) semipolar $(1\bar{1}01)$ GaN layers in comparison with *c*-plane GaN/sapphire template (curve 2) and state-of-the-art *c*-plane nano-ELO GaN templates (curve 4). Excitation density is 0.32 kW/cm^2. Numbers indicate values of slow decay component τ_2. Dashed curves represent the system response.

templates. The PL intensity for the coalesced layer is however lower by one order of magnitude, which may be attributed to defects formed in the layer as a result of coalescence and relatively larger total area of the defective c$^-$ wings. Figure 6(b) compares room temperature large area excitation TRPL spectra from the coalesced and non-coalesced semipolar layers on Si (001) and the two reference *c*-plane GaN layers. The normalized TRPL data were fit by using a biexponential decay function

$$A_1 \exp(-t/\tau_1) + A_2 \exp(-t/\tau_2), \quad (1)$$

where A_1 and A_2 are the amplitudes of the fast and slow decay components with representative time constants of τ_1 and τ_2, respectively. As seen from the figure, the slow decay component, representative of the radiative recombination, for the non-coalesced layer is as long as 1.98 ns, which is substantially longer than that for the conventional *c*-plane GaN layer on sapphire (0.62 ns) and even longer than that of the state-of-the-art nano-ELO GaN layer (1.16 ns). This long slow decay constant is indicative of high optical quality of the non-coalesced semipolar layer with low density of extended and point defects. Note that τ_2 for the coalesced layer is substantially shorter (0.20 ns). This conclusion is in a good agreement with the steady-state PL results presented in Fig. 6(a) showing one order of magnitude higher PL intensity for the non-coalesced layer comparing to the coalesced one.

Figures 7(a) and 7(b) show room-temperature excitation density dependent TRPL for the *c*-plane nano-ELO GaN and non-coalesced semipolar $(1\bar{1}01)$ GaN on Si(001) layers, respectively. Table I lists the biexponential fitting parameters for the PL transients for various excitation power densities. As seen from Fig. 7 and Table I, the fast component of the PL transients, τ_1, representative of the nonradiative

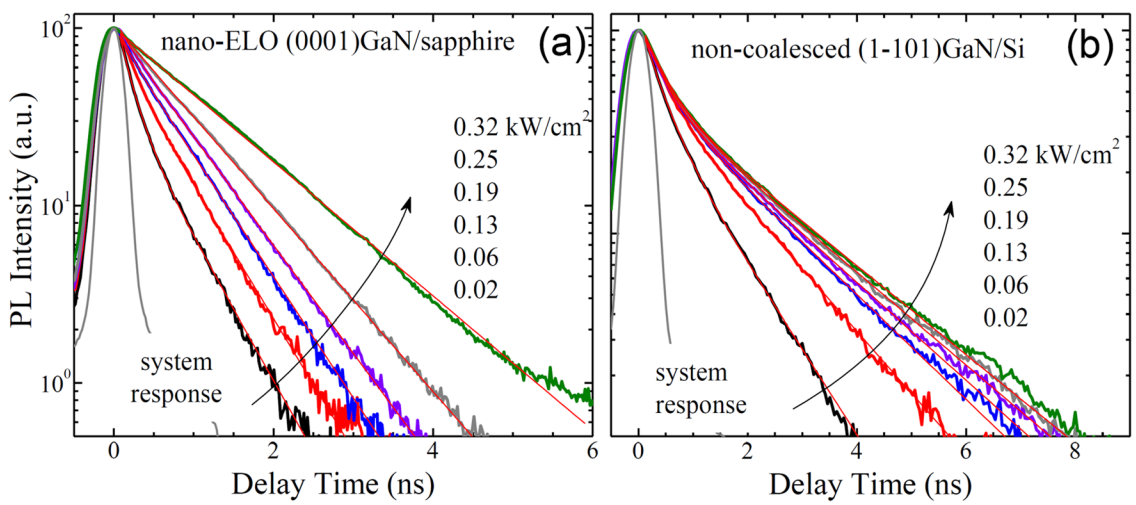

FIG. 7. Excitation density dependent room-temperature TRPL for (a) polar (0001) nano-ELO GaN film on sapphire and (b) semipolar non-coalesced $(1\bar{1}01)$GaN layer on Si.

TABLE I. PL decay times and amplitude ratios obtained from biexponential fits.

Excitation (kW/cm^2)	τ_1 (ns)	τ_2 (ns)	A_1/A_2
Polar *c*-plane nano-ELO film			
0.02	0.16	0.54	2.02
0.06	0.19	0.58	0.65
0.13	0.15	0.64	0.22
0.19	0.16	0.71	0.15
0.25	-	0.84	0
0.32	-	1.15	0
$(1\bar{1}01)$ non-coalesced layer			
0.02	0.33	1.03	1.38
0.06	0.38	1.42	1.12
0.13	0.38	1.68	1.10
0.19	0.38	1.80	1.11
0.25	0.39	1.90	1.17
0.32	0.40	1.98	1.19

recombination, is virtually independent of the excitation power density for both polar and semipolar GaN, while the slow decay component for both layers becomes longer with increasing excitation power density. However, the amplitude ratio A_1/A_2 for the polar and semipolar GaN samples varies with the excitation power density in different ways. For the polar GaN, the amplitude ratio A_1/A_2 decreases rapidly with increasing excitation power density, and the TRPL shows virtually single-exponential decay for the highest excitation power densities of 0.25 and 0.32 kW/cm^2. For the semipolar film, the amplitude ratio A_1/A_2 reduces only slightly with increasing excitation power density. This implies that the polar nano-ELO GaN contains relatively low concentration of nonradiative centers (point and/or extended defects); therefore, the nonradiative and the radiative recombination channels compete at low excitations, but radiative recombination becomes dominant at high excitation density due to limited number of nonradiative centers. To the contrary, as evident from higher A_1/A_2 ratio, within the excitation area, the number of nonradiative centers in semipolar GaN is larger; therefore, the nonradiative recombination channel contributes substantially even at high excitation power densities. In the case of $(1\bar{1}01)$ GaN, regions with very different structural quality contribute to the TRPL signal: high-quality c^+-wing regions, probably responsible for the long slow decay

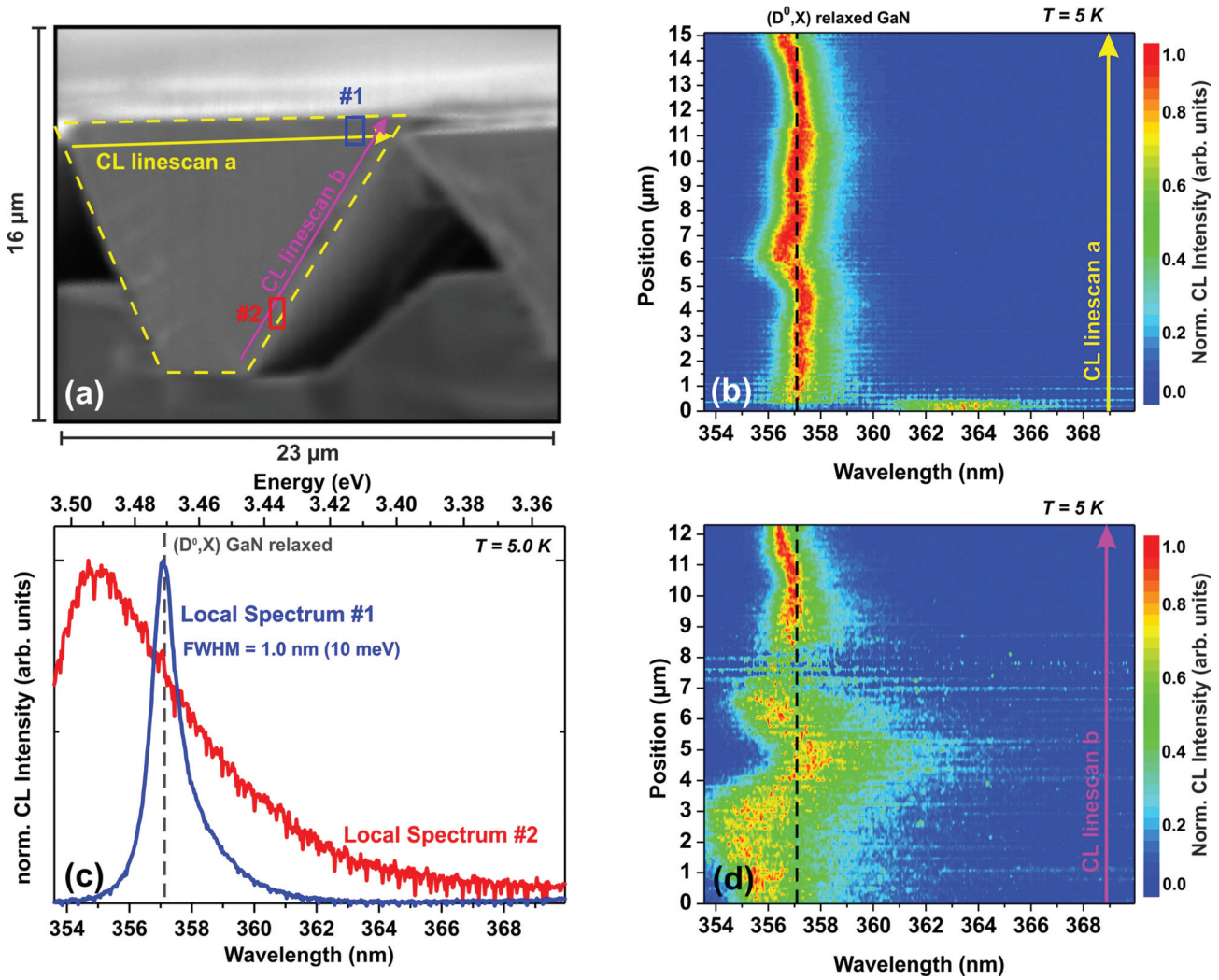

FIG. 8. (a) Cross-sectional SEM image of non-coalesced $(1\bar{1}01)$ GaN layer on Si (001); arrows show the directions of CL spectrum linescans performed (b) along the surface and (d) across the layer thickness. (c) Local CL spectra measured from near-surface (blue rectangle #1 in (a)) and near-bottom (red rectangle #2 in (a)) regions. Dashed lines in (b), (c), and (d) indicate the wavelength of (D^0, X) emission from relaxed GaN.

components τ_2, together with the portions of c^+-wings close to the GaN/Si(111) interface featured by high dislocation density and highly defective c^--wings, contributing to non-radiative decay that is mainly responsible for the fast decay components τ_1. It is apparent from the data in Fig. 7(b) that the contribution from defects present in the lower quality regions is essential even at high excitation densities.

C. Strain distribution in semipolar (1$\bar{1}$01) GaN

Upon cooling from the high growth temperature, the thermal-expansion mismatch between the Si substrate and the GaN film causes substantial strain in the epitaxial structure. To determine strain in our structures, CL linescans were performed along the surface and across the thickness of the non-coalesced and coalesced layers (Figs. 8 and 9, respectively). For the non-coalesced layer, the (D^0, X) emission wavelength shows only a minor variation along the surface and matches that of relaxed GaN [shown by dashed line in Fig. 8(b)], which suggests that the near-surface region is virtually free of strain. This is explained by the ease of strain relaxation in GaN stripes that have very limited contact with the Si substrate. The CL linescan measured across the thickness of the non-coalesced layer [Fig. 8(d)] shows a narrow line width in the near-surface region of the stripe (linescan position of 9-12μm) and significantly broadened peak at linescan positions $<8\,\mu$m. It should be mentioned that CL is sensitive to both strain and free carrier concentration in the material. Pure strain can result in a peak shift, but not in peak broadening, while increasing carrier concentration leads to the red shift due to band gap renormalization and then to the blue shift due to band filling, and to the peak broadening. Therefore, broadening and shifting of the CL peak from the bottom region should be related not only to strain, but also to increased concentration of free carries, presumably due to impurity incorporation from Si and/or SiO_2. We can presume that Si and/or O species diffuse fast along threading dislocations, which propagate along the c^+-direction from the Si/AlN/GaN interface to the surface [see Figs. 3(b) and 3(c)] and cross the CL linescan at positions below

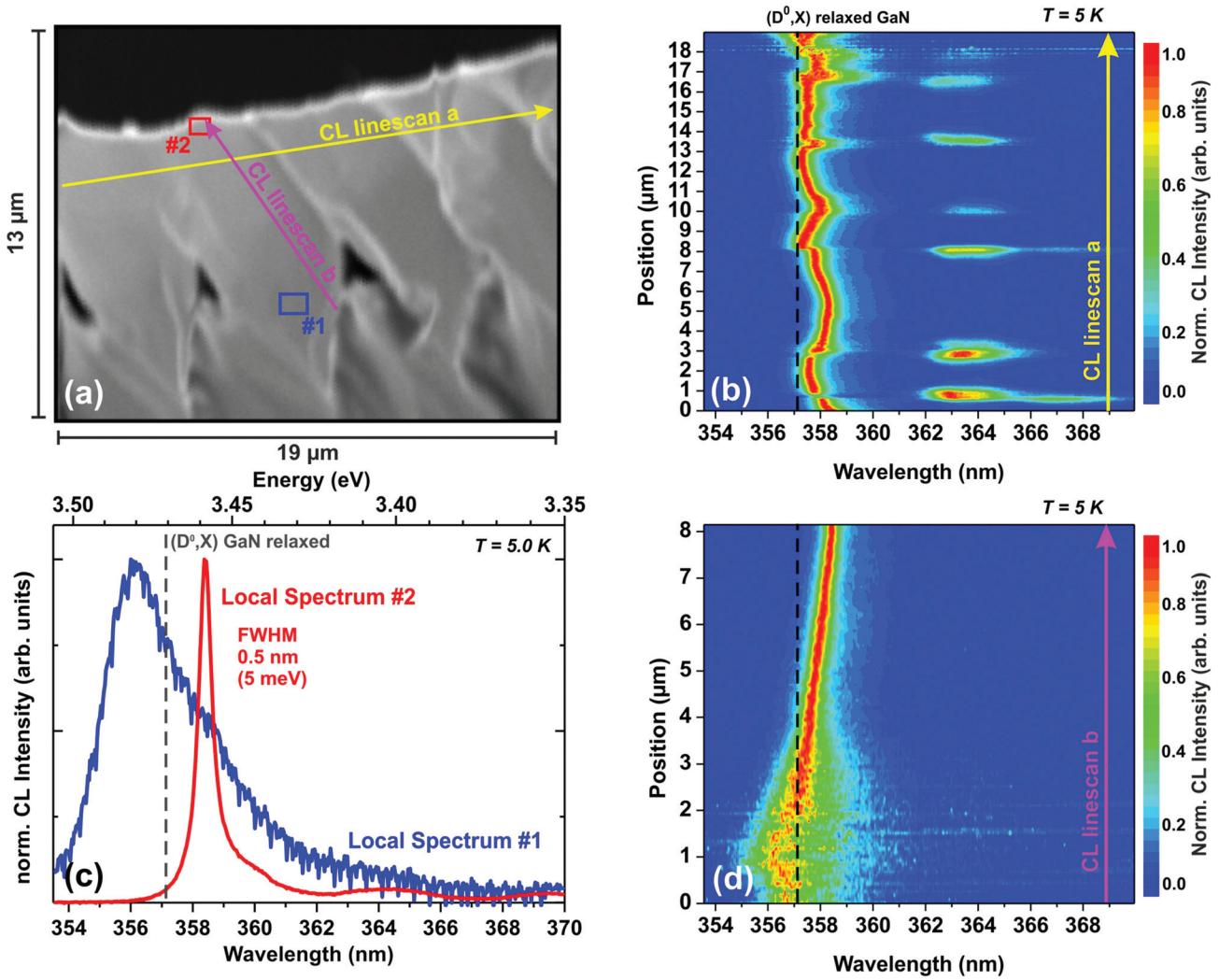

FIG. 9. (a) Cross-sectional SEM image of coalesced (1$\bar{1}$01) GaN layer on Si(001) (the images are slightly distorted due to charging effect during measurements); arrows show the directions of CL spectrum linescans performed (b) along the surface and (d) across the layer thickness. (c) Local CL spectra measured from near-surface (blue rectangle #1 in (a)) and near-bottom (red rectangle #2 in (a)) regions. Dashed lines in (b), (c), and (d) indicate the wavelength of (D^0, X) emission from relaxed GaN.

8 μm. As a result, at this bottom portion, a high level of incorporated impurities (Si and/or O, both acting as shallow donors in GaN) leads to a high concentration of free carriers broadening and shifting the CL peak spectrally.

Figure 9 shows the cross-sectional SEM image and the corresponding CL spectrum linescans across the coalesced film thickness and along the film surface. As seen from the CL spectrum linescan in Fig. 9(b), the strain distribution over the surface of the coalesced film is very inhomogeneous. The red shift of the NBE luminescence from the surface compared to relaxed GaN reaches 9 meV, which corresponds to a tensile stress of 0.3 GPa.[31] As in the case of the non-coalesced layer, the region near the GaN/AlN/Si (111) interface shows a slightly blue shifted and broadened NBE emission [Fig. 9(d)], which is indicative of a high concentration of free carriers due to incorporation of impurities like mask material.

It is not surprising that the strain level is substantially lower in the non-coalesced structure, since the non-coalesced GaN stripes are free to move in the direction perpendicular to the stripes, thus relaxing strain, while the coalesced layer is clamped to the substrate. It may be speculated that rather high strain level may be one of the reasons for the weaker luminescence emanating form the coalesced layer [see Fig. 6(a)], since highly strained regions should give rise to accumulation of point defects generated at the high growth temperature. The point defects and point defect complexes are known to act as non-radiative centers.

IV. CONCLUSIONS

Optical properties and defect distribution in the coalesced and non-coalesced $(1\bar{1}01)$ GaN layers grown by MOCVD on patterned Si substrates were studied. Spectrally and spatially resolved CL in combination with SEM images revealed that the c^+-wings are mainly free of stacking faults and thus dominated by the NBE emission, whereas a large density of BSFs exists in the c^- wings of the non-coalesced layers. As the growth proceeds and the c^+ and c^- fronts meet forming a continuous film, the existing BSFs continue to propagate in the direction perpendicular to the c-axis reaching the film surface. BSFs were also found within c^+ wings of the coalesced layer, in the regions where the c^+ wings contact with the SiO_2 masking layer. The origin of these BSFs may be attributed to oxygen/silicon out-diffusion and/or strain concentration in the near-contact region. No optically active defects were found at the coalescence boundaries. CL line scans along the surface and across the thickness of non-coalesced and coalesced layers revealed that the near-surface region of non-coalesced layers is relaxed, and coalescence results in nonuniform strain distribution across the surface. The near-surface regions of the coalesced layer are under tensile stress of up to 0.3 GPa. Blue shifted and broadened NBE emission observed from the regions near the GaN/AlN/Si (111) interface is indicative of a high concentration of free carriers presumably due to incorporation of shallow-donor impurities (Si and/or O) from the substrate. The steady-state and time-resolved PL data indicate that semipolar $(1\bar{1}01)$GaN on patterned Si exhibits high optical performance, in terms of PL intensity and carrier lifetimes ($\sim$2 ns), approaching that of the state-of-the-art c-plane GaN grown using *in situ* SiN_x nanonetwork mask on c-plane sapphire. In aggregate, the findings suggest that the semipolar material has great potential for light emitting and detecting devices.

ACKNOWLEDGMENTS

The work at VCU was funded by the National Science Foundation (Project Nos. DMR # 0907096 and DMR #1210282 under direction of Dr. Ch. Ying). The work at Magdeburg University was funded by the German Research Foundation DFG in the frame of the research unit FOR 957 "PolarCoN."

[1]A. A. Berg and P. J. Dean, *Light-Emitting Diodes* (Clarendon, Oxford, 1976), pp. 11–35.
[2]H. Morkoç, *Handbook of Nitride Semiconductors and Devices* (Wiley-VCH, 2008–2009).
[3]R. Langer, J. Simon, V. Ortiz, N. T. Pelekanos, A. Barski, R. Andre, and M. Godlewski, Appl. Phys. Lett. **74**, 3827 (1999).
[4]T. Deguchi, K. Sekiguchi, A. Nakamura, T. Sota, R. Matsuo, S. Chichibu, and S. Nakamura, Jpn. J. Appl. Phys., Part 2 **38**, L914 (1999).
[5]M. Zamfirescu, B. Gil, N. Grandjien, G. Mapluech, A. Kavokin, P. Bigenwald, and J. Massies, Phys. Rev. B **64**, 121304 (2001).
[6]T. Takeuchi, H. Amano, and I. Akasaki, Jpn. J. Appl. Phys., Part 1 **39**, 413 (2000).
[7]T. J. Baker, B. A. Haskell, F. Wu, P. T. Fini, J. S. Speck, and S. Nakamura, Jpn. J. Appl. Phys., Part 2 **44**, L920–L922 (2005).
[8]J. Baker, B. A. Haskell, F. Wu, J. S. Speck, and S. Nakamura, Jpn. J. Appl. Phys., Part 2 **45**, L154 (2006).
[9]X. Ni, Ü. Özgür, A. A. Baski, H. Morkoç, L. Zhou, D. J. Smith, and C. A. Tran, Appl. Phys. Lett. **90**, 182109 (2007).
[10]M. Funato, M. Ueda, Y. Kawakami, Y. Narukawa, T. Kosugi, M. Takahashi, and T. Mukai, Jpn. J. Appl. Phys., Part 2 **45**, L659 (2006).
[11]T. Matsubara, R. Senda, D. Iida, M. Iwaya, S. Kamiyama, H. Amano, and I. Akasaki, J. Cryst. Growth **311**, 2926–2928 (2009).
[12]N. Sawaki, T. Hikosaka, N. Koide, S. Tanaka, Y. Honda, and M. Yamaguchi, J. Cryst. Growth **311**, 2867 (2009).
[13]N. Izyumskaya, S. J. Liu, S. Okur, M. Wu, V. Avrutin, Ü. Özgür, S. Metzner, F. Bertram, F. Bertram, L. Zhou, D. J. Smith, and H. Morkoç, Proc. SPIE **7939**, 79391W (2011).
[14]N. P. Hylton, P. Dawson, C. F. Johnston, M. J. Kappers, J. L. Hollander, C. McAleese, and C. J. Humphreys, Phys. State Solidi C **6**, S727 (2009).
[15]M. Feneberg, F. Lipski, R. Sauer, K. Thonke, T. Wunderer, B. Neubert, P. Brückner, and F. Scholz, Appl. Phys. Lett. **89**, 242112 (2006).
[16]H. Masui, H. Asamizu, T. Melo, H. Yamada, K. Iso, S. C. Cruz, S. Nakamura, and S. P. DenBaars, J. Phys. D **42**, 135106 (2009).
[17]S. Nakamura, "The latest performance of GaN-based nonpolar and semipolar emitting devices," in Proceedings of 69th Annual Device Research Conference (DRC), Santa Barbara, CA, June 2011.
[18]H. Masui, S. Nakamura, S. P. DenBaars, and U. K. Mishra, IEEE Trans. Electron Devices **57**, 88 (2010).
[19]Z. Liliental-Weber, J. Jasinski, and D. N. Zakharov, Opto-Electron. Rev. **12**, 339 (2004).
[20]R. M. Farrell, E. C. Young, F. Wu, S. P. DenBaars, and J. S. Speck, Semicond. Sci. Technol. **27**, 024001 (2012).
[21]Y. Honda, N. Kameshiro, M. Yamaguchi, and N. Sawaki, J. Cryst. Growth **242**, 82 (2002).
[22]X. Ni, M. Wu, J. Lee, X. Li, A. A. Baski, Ü. Özgür, and H. Morkoç, Appl. Phys. Lett. **95**, 111102 (2009).
[23]N. Izyumskaya, S. J. Liu, V. Avrutin, S. Okur, Ü. Özgür, S. Metzner, C. Karbaum, F. Bertram, J. Christen, D. J. Smith, and H. Morkoç, Proc. SPIE **8262**, 826224 (2012).
[24]J. Xie, Ü. Özgür, Y. Fu, X. Ni, H. Morkoç, C. K. Inoki, T. S. Kuan, J. V. Foreman, and H. O. Everitt, Appl. Phys. Lett. **90**, 41107 (2007).

[25]F. Bertram, T. Riemann, J. Christen, A. Kaschner, A. Hoffmann, C. Thomsen, K. Hiramatsu, T. Shibata, and N. Sawaki, Appl. Phys. Lett. **74**, 359 (1999).
[26]K. Motoki, T. Okahisa, S. Nakahata, N. Matsumoto, H. Kimura, H. Kasai, K. Takemoto, K. Uematsu, M. Ueno, Y. Kumagai, A. Koukitu, and H. Seki, J. Cryst. Growth **237–239**, 912 (2002).
[27]R. Liu, A. Bell, F. A. Ponce, C. Q. Chen, J. W. Yang, and M. A. Khan, Appl. Phys. Lett. **86**, 021908 (2005).
[28]P. P. Paskov, R. Schifano, B. Monemar, T. Paskova, S. Figge, and D. Hommel, J. Appl. Phys. **98**, 093519 (2005).
[29]N. Izyumskaya, S. J. Liu, V. Avrutin, X. F. Ni, M. Wu, Ü. Özgür, S. Metzner, F. Bertram, J. Christen, L. Zhou, D. J. Smith, and H. Morkoç, J. Cryst. Growth **314**, 129 (2011).
[30]A. Dadgar, R. Ravash, P. Veit, G. Schmidt, M. Mueller, A. Dempewolf, F. Bertram, M. Wieneke, J. Christen, and A. Krost, Appl. Phys. Lett. **99**, 021905 (2011).
[31]C. Kisielowski, J. Krüger, S. Ruvimov, T. Suski, J. W. Ager III, E. Jones, Z. Liliental-Weber, M. Rubin, E. R. Weber, M. D. Bremser, and R. F. Davis, Phys. Rev. B **54**, 17745 (1996).